Published in final edited form as:
Skeletal Radiol. 2013 July ; 42(7): 1007–1010. doi:10.1007/s00256-013-1594-7.

Plexiform nerve sheath tumor or vascular malformation—role of advanced MR neurography and diffusion tensor imaging

Sahar Jalali-Farahani,
Russell H Morgan Department of Radiology & Radiological Science, 601 N. Caroline St, JHOC 3262, Baltimore, MD 21287, USA

Jaishri O. Blakeley,
Department of Neurology, Johns Hopkins School of Medicine, Baltimore, MD, USA

Allan J. Belzberg,
Department of Neurosurgery, Johns Hopkins School of Medicine, Baltimore, MD, USA

John A. Carrino, and
Russell H Morgan Department of Radiology & Radiological Science, 601 N. Caroline St, JHOC 3262, Baltimore, MD 21287, USA

Avneesh Chhabra
Russell H Morgan Department of Radiology & Radiological Science, 601 N. Caroline St, JHOC 3262, Baltimore, MD 21287, USA, Department of Radiology, Johns Hopkins School of Medicine, Baltimore, MD, USA

Avneesh Chhabra: achhabr6@jhmi.edu

Abstract

The authors report a vascular malformation mimicking a plexiform peripheral nerve sheath tumor. Three Tesla magnetic resonance neurography with high-resolution anatomic and advanced functional diffusion tensor imaging was helpful in evaluating full extent of the lesion and characterizing its internal architecture.

Keywords

Vascular Malformation; Magnetic Resonance Neurography; Nerve Sheath Tumor

Case report

A 51-year-old woman with a past history of hypercholesterolemia and osteoporosis presented at an outside institution with recent complaints of headaches, palpitations, dull shoulder pain, sensory symptoms of tightness, and burning pain in the upper and lower

Correspondence to: Avneesh Chhabra, achhabr6@jhmi.edu.

Financial disclosure statement Dr. Carrino has received patient research grants from Siemens and Toshiba. Dr. Chhabra has received patient research grants on MR Neurography from Siemens, Integra Life Sciences, and GE-AUR. Dr. Chhabra also serves as a MSK consultant with Siemens CAD division unrelated to this research.

limbs. She was evaluated by conventional MR imaging of head and cervical spine and no acute finding was noted in brain or cervical spine. However, she was found to have a plexiform mass in the left shoulder region, suspected to be due to neurofibromatosis type 1 (NF1). Three months later, for further evaluation, she visited Johns Hopkins Comprehensive Neurofibromatosis Center. She further reported that there had been heaviness in her shoulder for many months, which had exacerbated in the last 2 months. She did not report a family history of NF1. The physical examination revealed fullness in the left supraspinatus, rhomboid, and axillary regions without a focal palpable mass. Three 'Café au lait'-like spots were noted in the posterior left arm, anterior left arm, and right forearm; none of them met the standard criteria for NF1, as all were smaller than 1.5 cm. There were no cutaneous neurofibromas or Lisch nodules. The muscle strength of all four limbs was normal along with normal deep tendon reflexes and sensory examination. The patient was counseled for possible future genetic studies and in the meantime, high-resolution MR neurography (MRN) of the left upper extremity and brachial plexus on a high-field, 3-Tesla scanner (Verio, Siemens, Erlangen, Germany) was ordered to further characterize the mass lesion. The imaging included two-dimensional (2D) and isotropic 3D anatomic imaging, post-gadolinium isotropic 3D post-intravenous contrast T1-weighted imaging, as well as functional, diffusion tensor imaging (DTI). The anatomic imaging included axial T1-weighted (repetition time, TR: 961 ms; echo time, TE: 9.4 ms; slice, SL: 6 mm; base resolution, BR; 320), axial T2-weighted Spectral adiabatic inversion recovery (SPAIR) (TR: 3,600 ms; TE: 71 ms; SL: 6 mm; BR; 320) and 3D Short tau inversion recovery sampling perfection with application-optimized contrasts using varying flip-angle evolutions (STIR-Space, Siemens, Erlangen, Germany) (TR: 1,500 ms; TE: 84 ms; SL: 1.2 mm; BR; 384).

The anatomic MRN imaging revealed a large plexiform isointense lesion on T1-weighted and hyperintense lesions on T2-weighted images involving the left brachial plexus, enveloping the nerve roots to the terminal branches and extending into the superolateral aspect of the left chest wall. Three-dimensional imaging showed the full extent of the lesion, both anteriorly and posteriorly, although the lesion was poorly differentiated from the adjacent brachial plexus due to similar hyperintensity of the regional nerves and the infiltrative lesion. The subclavian artery, left axillary, and brachiocephalic veins remained patent. Post-contrast images demonstrated focal enhancement along the anterolateral chest wall with the appearance of a small vascular tangle, while most portions of the lesion showed poor to no enhancement indicating cystic contents (Fig. 1).

DTI (functional imaging) (TR: 5,621 ms; TE: 80 ms; SL: 5 mm; BR; 98) was performed using two diffusion moments (0 and 600 s/mm^2) and 20 directions of gradient interrogation. The lesion was best seen on the tensor and apparent diffusion coefficient (ADC) maps, and showed poor diffusion restriction with high apparent diffusion coefficient values (1.8–1.9 × 10−3 mm/s^2). It showed uniform hyperintensity on the diffusion images due to T2 shine through artifact. The tensor map projection image could distinguish the brachial plexus from the lesion (Fig. 2) and the visualized, partially included right brachial plexus was also normal. The fractional anisotropy map showed poor to no visualization of the lesion while nicely showing the spinal cord and the left brachial plexus, confirming lack of anisotropy within the lesion. These findings therefore suggested a vascular malformation with predominant cystic components rather than a nerve sheath tumor [1–3]. Since the MRN

examination did not include dynamic contrast-enhanced imaging, a duplex Doppler ultrasound (USG) examination was ordered to detect any possible flow in the lesion. USG showed hypo-anechoic subcutaneous lesion with marked through transmission, confirming the cystic nature of the lesion (not shown). It did not depict vascular signals within the lesion on Doppler images consistent with lack of solid component [4, 5]. The chest wall MR-enhancing component was not detected on USG due to its deep location. A final diagnosis of venolymphatic malformation was established based on high-resolution MRN and USG findings and no further genetic work-up was warranted.

Discussion

Venolymphatic malformation is a mixed-type, slow-flow vascular anomaly, which can be congenital or acquired due to trauma. The congenital form can present at the birth or the diagnosis may be delayed for weeks to years after the birth. The lesions might become symptomatic with increasing age, and may present with symptoms of heaviness, mass effect, or pain, as seen in our case. Conventional MRI has been used in its evaluation and shows the lesions as hyperintense lobules on T2-weighted images with/without focal hypointense phleboliths [3, 6, 7]. The cavernous portions enhance with intravenous contrast without arteriovenous shunting on dynamic MR imaging [8]. However, a large infiltrative vascular lesion without phleboliths can easily mimic a plexiform nerve sheath tumor and may lead to extensive diagnostic work-up, such as multiple imaging studies, needle interventions, and genetic work-up, especially when the vascular malformation is not initially suspected and dynamic contrast MR imaging is not available [8, 9].

Three Tesla MRN is a helpful technique as it can show the full extent of the lesion and reveal both vascular (enhancing) and lymphatic (non-enhancing) components due to intrinsic high soft-tissue contrast and resolution. However, either dynamic contrast imaging or USG are needed for assessment of presence and type of internal vascularity [8–10]. Anatomic MRN can show the full extent of the lesion in multiple planes, is more objective than USG, and finally can detect deep portions of the lesion (venous component in our case); however, it may be difficult to delineate a large infiltrative lesion separately from the brachial plexus nerves due to the similar signal characteristics of nerves and adjacent slow-flow vessels. DTI adds another dimension to the anatomic MRN, as it shows the otherwise inconspicuous internal characteristics of the lesion as well as may help differentiate the nerves from surrounding pathology due to the ability of DTI to interrogate functional/micro-architectural proton diffusion characteristics [11, 12]. As shown in our case, it confirms the high diffusivity as well as lack of anisotropy expected within the cystic lesion. Due to the highly organized fascicular structure of the nerves, there is considerable anisotropic diffusion of protons within the normal nerves, and therefore, DTI shows the nerves separate from the infiltrative lesion. It has the potential to replace intravenous contrast imaging, however that remains to be tested.

To conclude, plexiform appearing mass lesions can result in clinical and imaging diagnostic dilemma. High resolution MRN imaging with DTI can not only depict the entire extent of the lesion but also aid in accurate imaging characterization leading to diagnosis for appropriate patient management.

References

1. Fishman SJ, Mulliken JB. Hemangiomas and vascular malformations of infancy and childhood. 6. Pediatr Clin North Am. 1993; 40:1177–200. [PubMed: 8255621]
2. Baker LL, Dillon WP, Hieshima GB, Dowd CF, Frieden IJ. Hemangiomas and vascular malformations of the head and neck: MR characterization. 2. AJNR Am J Neuroradiol. 1993; 14:307–14. [PubMed: 8456703]
3. Suh JS, Hwang G, Hahn SB. Soft tissue hemangiomas: MR manifestations in 23 patients. 8. Skeletal Radiol. 1994; 23:621–5. [PubMed: 7886471]
4. Vaišnytė B, Vajauskas D, Palionis D, Misonis N, Kurminas M, Nevidomskytė D, et al. Diagnostic methods, treatment modalities, and follow-up of extracranial arteriovenous malformations. Med (Kaunas). 2012; 48(8):388–98.
5. Niu ZB. Retroperitoneal lymphatic malformation in child with horseshoe kidney. Urology. 2012; 79(2):437–9. [PubMed: 21908028]
6. Rak KM, Yakes WF, Ray RL, Dreisbach JN, Parker SH, Luethke JM, et al. MR imaging of symptomatic peripheral vascular malformations. 1. AJR Am J Roentgenol. 1992; 159:107–12. [PubMed: 1609682]
7. Flors L, Leiva-Salinas C, Maged IM, et al. MR imaging of soft-tissue vascular malformations: diagnosis, classification, and therapy follow-up. Radiographics. 2011; 31(5):1321–40. [PubMed: 21918047]
8. Lidsky ME, Spritzer CE, Shortell CK. The role of dynamic contrast-enhanced magnetic resonance imaging in the diagnosis and management of patients with vascular malformations. J Vasc Surg. 2012; 56(3):757–64. e1. [PubMed: 22840741]
9. Ohgiya Y, Hashimoto T, Gokan T, et al. Dynamic MRI for distinguishing high-flow from low flow peripheral vascular malformations. AJR Am J Roentgenol. 2005; 185(5):1131–7. [PubMed: 16247121]
10. Chhabra A, Lee PP, Bizzell C, Soldatos T. 3 Tesla MR neurography–technique, interpretation, and pitfalls. Skeletal Radiol. 2011; 40(10):1249–60. [PubMed: 21547613]
11. Vargas MI, Viallon M, Nguyen D, et al. New approaches in imaging of the brachial plexus. Eur J Radiol. 2010; 74(2):403–10. [PubMed: 20223611]
12. Chhabra A, Thakkar RS, Andreisek, et al. Anatomic MR imaging and functional diffusion tensor imaging of peripheral nerve tumor and tumor like conditions. AJNR Am J Neuroradiol. 2012 Nov 1. Epub ahead of print.

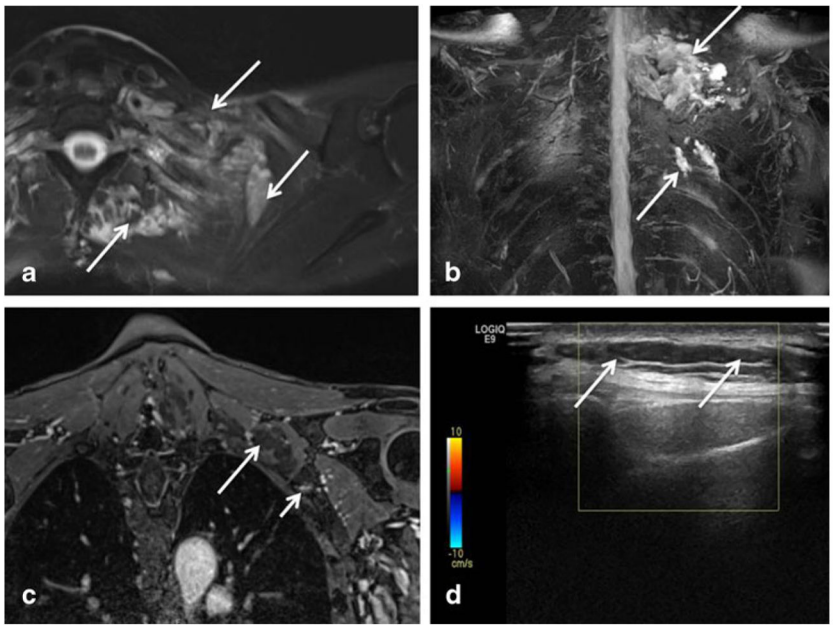

Fig 1.

a–d Axial T2 SPAIR (**a**), coronal 3D maximum intensity projection (MIP) STIR SPACE (**b**), coronal post-contrast 3D fat-suppressed T1W (**c**), and axial grey scale (**d**) ultrasound images of the left lower neck and shoulder. Note T2 hyperintense plexiform lesion (*arrows* in **a** and **b**) inseparable from the left brachial plexus segments, mimicking a plexiform peripheral nerve sheath tumor. The lesion showed no to poor enhancement in its most part (*large arrow* in **c**). Only a small tangle of vascular enhancement was noted (*small arrow* in **c**). Ultrasound image (**d**) shows the cystic nature again with marked through transmission posterior enhancement (*arrows*) and no flow on color Doppler

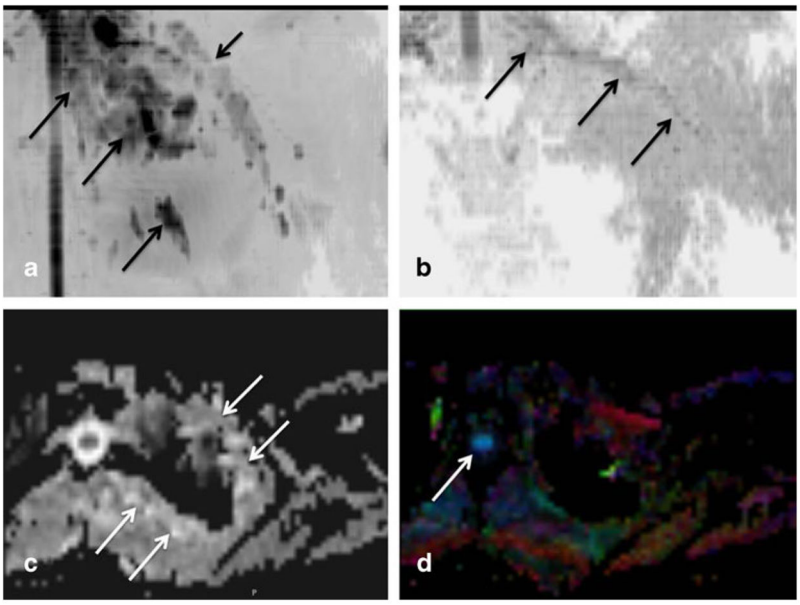

Fig 2.

a–d Functional diffusion tensor imaging (DTI). Coronal inverted scale MIP diffusion tensor image (**a**), coronal inverted scale MIP fractional anisotropy (FA) image (**b**), axial grey scale apparent diffusion coefficient (ADC) image (**c**) and axial color FA map image (**d**) of the left lower neck and shoulder. There is a good depiction of the lesion on tensor map (*large arrows* in **a**) as well as its relative separation from the left brachial plexus nerves (*small arrow* in **a**). Note selective depiction of the brachial plexus nerves on FA map (*arrow* in **b**) due to good anisotropy created by myelin sheaths and fascicular architecture of the nerves. Axial images show the lesion on ADC map (*arrows* in **c**) due to artifactual T2 shine through but the lesion is not seen on colored FA map (**d**). Good depiction of spinal cord is noted (*arrow* in **d**) due to relative structural organization leading to anisotropy